

Soft Matter

Accepted Manuscript



This is an *Accepted Manuscript*, which has been through the Royal Society of Chemistry peer review process and has been accepted for publication.

Accepted Manuscripts are published online shortly after acceptance, before technical editing, formatting and proof reading. Using this free service, authors can make their results available to the community, in citable form, before we publish the edited article. We will replace this *Accepted Manuscript* with the edited and formatted *Advance Article* as soon as it is available.

You can find more information about *Accepted Manuscripts* in the [Information for Authors](#).

Please note that technical editing may introduce minor changes to the text and/or graphics, which may alter content. The journal's standard [Terms & Conditions](#) and the [Ethical guidelines](#) still apply. In no event shall the Royal Society of Chemistry be held responsible for any errors or omissions in this *Accepted Manuscript* or any consequences arising from the use of any information it contains.

Understanding and overcoming shear alignment of fibers during extrusion

Joshua J. Martin^a, Michael Riederer^b, Melissa Krebs^b, and Randall M. Erb^{*a}

Fiber alignment is the defining architectural characteristic of discontinuous fiber composites and is dictated by shear-dominated processing techniques including flow-injection molding, tape-casting, and mold-casting. However, recent colloidal assembly techniques have started to employ additional forces in fiber suspensions that have the potential to change the energy landscape of the shear-dominated alignment in conditions of flow. In this paper, we develop an energetics model to characterize the shear-alignment of rigid fibers under different flow conditions in the presence of magnetic colloidal alignment forces. We find that these colloidal forces can be sufficient to manipulate the energetic landscape and obtain tunable fiber alignment during flow within even small geometries, such as capillary flow. In most conditions, these colloidal forces work to freeze the fiber orientation during flow and prevent the structure disrupting phenomenon of Jeffrey's orbits that has been accepted to rule fiber suspensions under simple shear flow.

Introduction

While continuous-fiber composites (CFCs) are typically reserved for high-performance structures, discontinuous-fiber composites (DFCs) are much cheaper to produce, can be used to obtain complex geometries, and can even approach the mechanical properties of CFCs if the fibers are well aligned in the direction of the principal applied stress.¹ Fiber architecture (i.e. the spatial distribution and alignment of fibers within a matrix material) plays a critical role in the bulk mechanical properties of a fabricated structure.² Common shear lag composite theory suggests that fibers oriented in the direction of the principal stresses will increase the strength of the composite provided there exists strong interaction between the fiber and the matrix.³ However, fibers that are oriented perpendicular to the applied stress will actually work to decrease the overall mechanical strength of the material.⁴

As orientation of fibers within a composite is one of the most significant factors that defines the strength of the ultimate structure, composite processing technologies are focused upon maximizing fiber alignment in the direction of the principal stress.⁵ One of the dominating orienting forces in composite melts and precursors solutions is shear. Shear forces have been investigated and employed to enhance fiber alignment and improve composite mechanical properties.^{6, 7} Shear alignment is dominant in processes such as injection molding, extrusion, compression molding and tape-casting.²

In these processes, the geometry of the device or of the mold dictates the alignment of these high-aspect ratio fibers independent of the user's preferred orientation that would maximize composite performance. Undesired alignment in injection molding is combatted with significant effort placed on mold design to determine flow injection ports and streamlines that provide the best (but not ideal) fiber architectures. Even in simple geometries like the cross-section of a cylindrical pipe, extrusion processes are complicated by shear-derived phenomena such

as Jeffrey orbits.⁸ This phenomenon causes a fiber to continuously rotate during extrusion resulting in a randomized fiber architecture. These Jeffrey orbits are also known to result in poor alignment of fibers within tape-casted composites.⁹

Limiting processing techniques to shear orientation is not required as additional colloidal forces can be applied to limit or possibly even overcome the dominating effects of shear. This work employs colloidal magnetic forces provide an additional handle to both measure and combat these shear energies. These magnetic forces are obtainable with common nonmagnetic reinforcing fibers of specific geometries by first absorbing nominal amounts of magnetic nanoparticles to their surface such that they exhibit an ultra-high magnetic response.¹⁰ Though shear energies still tend to dominate many flow situations, this additional force can manipulate the average orientation and even completely arrest the phenomena of Jeffrey orbits that complicate composite processing technologies.

Presented here is an energetics model for aligning fibers in a shear flow by combining slender body theory with a magnetic alignment model. The derived analytic expression is demonstrated to predict fiber orientation across a series of flow configurations including different viscosities, flow rates, and field strengths. Finally, the ability to arrest Jeffrey orbits during extrusion processes to reach better alignments than standard flow conditions is shown.

Theory of fiber alignment

The effect of shear flow on the behavior of particles has been widely studied in the context of composites and complex colloidal systems¹¹. Shear forces have been shown to play critical roles in fiber suspensions as well as isotropic-nematic phase transitions in suspensions of rod-like viruses¹². The motion of a single ellipsoid immersed in a Newtonian fluid under simple shear flow was first solved theoretically by Jeffery et al in 1922.⁸ It was found that the rotation of the ellipsoid depends on the

fiber aspect ratio, $p = A/B$ where A and B are the long and short axis radii, respectively (Fig. 1a and b).

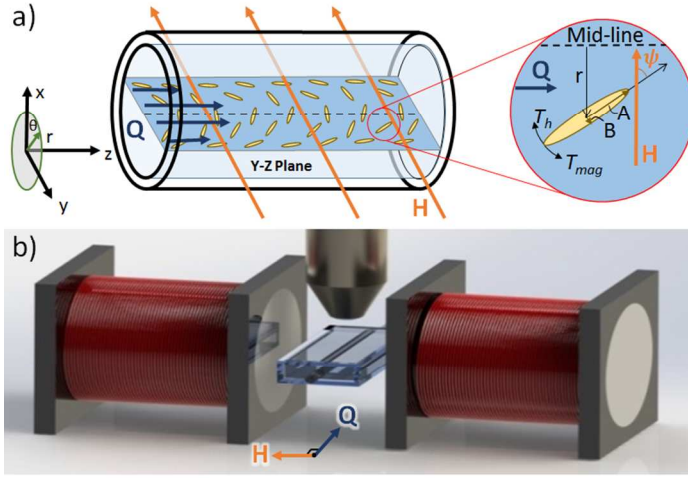


Fig. 1. a) Schematics of extrusion setup with key geometric variables defined for the flow conditions, magnetic field, and for a single fiber. b) The flow setup is depicted for experimental observation.

Jeffery orbits describe the periodic rotation of an ellipsoid suspended in a sheared fluid. This theory was expanded to particles of various cross sectional geometries in Stokes flow by Cox et al.^{13, 14} and Batchelor et al.^{15, 16} and later made applicable to all axisymmetric particles such as chopped fibers by Bretherton et al.¹⁷ In general, anisotropic particles will experience orbital motion along axes with asymmetric flow conditions due to a shear stress profile that leads to non-static particle alignment.

A prolate ellipsoid with a magnetic coating of thickness d will have a tendency to align in the flow direction undergoing Jeffrey orbits due to an applied shear and a tendency to orient its long axis in the direction of the applied magnetic field. The ellipsoid will reach an equilibrium orientation when the shear torque balances with the magnetic torque. Interpreting long fibers as prolate ellipsoids will allow analytical expressions to be employed for the magnetic energy as validated by Ooi et al.¹⁸ for fibers with large anisotropies. $p > 10$. The magnetic torque of a particle shell can be derived from the magnetic energy equation (1):

$$U_{mag} = -\frac{2\pi\mu_o\chi_{ps}^2}{3(\chi_{ps}+2)}[(A+d)(B+d)^2 - AB^2]H_o^2\sin^2\psi \quad (1)$$

Here μ_o is the permeability of free space ($\mu_o = 4\pi \cdot 10^{-7}$, units of $[N/A^2]$), χ_{ps} is the volume susceptibility of the particles (dimensionless), H_o is the external magnetic field (units of $[A/m]$), and ψ is the angle of the long axis of the particle to the vertical axis. The magnetic torque can then be derived from $T_{mag} = -dU_{mag}/d\psi$. This yields:

$$T_{mag} = \frac{4\pi\mu_o\chi_{ps}^2}{3(\chi_{ps}+2)}[(A+d)(B+d)^2 - AB^2]H_o^2\sin\psi\cos\psi \quad (2)$$

Meanwhile, the shear rate profile of a pipe with a circular cross-section can be found by taking the derivative of the velocity profile, leading to:

$$\dot{\gamma} = (8v_{max}r/D^2) \quad \text{where } v_{max} = 8Q/\pi D^2 \quad (3)$$

Here Q is the volumetric flow rate, D is the diameter of the conduit, and v_{max} is the maximum velocity at the centroid of the conduit. In this geometry, the long axis of the conduit and the direction of flow is taken to be in \hat{z} and the shear rate changes perpendicular to the flow in \hat{r} . Proceeding with a Newtonian fluid, where the viscosity (η) is independent of $\dot{\gamma}$, the hydrodynamic torque experienced by the fiber can be calculated using the slender body theory of Batchelor (1970) for the dilute regime (assuming no particle-particle interactions)¹⁹:

$$T_h = \frac{8\pi A^3 f^\perp}{3\ln(2p)}\eta\dot{\gamma}\cos^2\psi \quad (4)$$

Here, f^\perp is the geometric friction factor that can be found using:

$$f^\perp = (1 + 0.64/\ln(2p))/(1 - 0.5/\ln(2p)) \quad (5)$$

For non-Newtonian fluids, a power-law equation can be used in Eq. 4 to account for shear-rate dependent viscosities. The expressions for shear rate and hydrodynamic torque can be combined, leading to an applied torque due to the fluid as a function of the fiber's geometry, the angle of the fiber (ψ), the flow properties, and the distance from the center of the pipe (r). For example, for the y - z plane (observed in this work) the hydrodynamic torque is:

$$T_h = \frac{64\pi A^3 f^\perp}{3\ln(2p)}\frac{\eta v_{max}}{D^2}y\cos^2\psi \quad (6)$$

There will be three force components: two tangential force components will apply torque to spin the particle (Jeffrey orbits) and a translational force that will act to move the particle in r . Neglecting gravitational forces, a torque balance will naturally form at the orientation where the hydrodynamic torque is small enough to be stabilized by the magnetic torque. At this equilibrium orientation:

$$T_{Hydrodynamic} = -T_{Magnetic} \quad (7)$$

For the case where H_o is in the direction of $\theta = -\pi/2$, (as depicted in Fig. 1A). Solving for the equilibrium fiber angle (ψ_o) on the y - z plane yields:

$$\psi_o = \tan^{-1}[(-\alpha\beta y)] \quad (8)$$

$$\text{with } \alpha = \frac{A^3 f^\perp}{\ln(2p)(A+d)(A/p+d)^2 - A^3/p^2} \quad \text{and } \beta = \frac{16(\chi_{ps}+2)\eta v_{max}}{H_o^2\mu_o\chi_{ps}^2 D^2}$$

This expression can be used to determine the equilibrium alignment angle as a function of particle length, susceptibility, and position within a pipe for given flow conditions and an applied magnetic field. In Eq. 8, α represents the individual fibers geometric variables while β

represents the general conditions all rods experience within the capillary.

Materials and methods

Magnetized Calcium Phosphate Micro-rods

Calcium phosphate (CaP) rods were prepared according to a protocol modified from Zhang et al.²⁰ Aqueous solutions of 42 mM calcium and 25 mM phosphate were prepared by dissolving $\text{Ca}(\text{NO}_3)_2 \cdot 4\text{H}_2\text{O}$ and $(\text{NH}_4)_2\text{HPO}_4$ in 50 mM HNO_3 with 1 M acetamide. The pH was adjusted to 3.0 with ammonium hydroxide or 0.1 M HNO_3 . Hydrothermal precipitation was conducted in 125 mL aliquots contained in borosilicate glass bottles (Wheaton) autoclaved at 134° C for 15 hours. The precipitated rods were filtered with a fritted funnel, rinsed with dH_2O , and oven dried at 80° C before storing at room temperature.

To magnetize the rods, 375 μL of superparamagnetic iron oxide nanoparticles (EMG 705, 3.9 % vol Fe_3O_4 , Ferrotec.) are mixed with 10 grams of CaP in 200 mL of deionized water and stirred overnight. A negatively charged ligand-coating on the iron oxide allows the nanoparticles to electrostatically adsorb to the surface of the CaP fibers. A superconducting quantum interference device (SQUID) was used to characterize the magnetic susceptibility of the fiber assemblies. The susceptibility of the magnetic shell (χ_{ps}) on the fibers was calculated by taking the average of measurements from the SQUID and theoretical calculations using the number of fibers and Fe_3O_4 particles in solution (see supplementary material). The surface coating of the fibers was calculated to be 20%, leading to an χ_{ps} of 2.8. The fibers were suspended in glycerol (Sigma) and isobornyl acrylate (IBOA, Sigma).

Flow Setup to Observe Fibers in Applied Fields

The experimental flow setup (Fig. 1b) consists of a 1 mm diameter glass capillary submerged in a solution of sugar water (65% wt.) in order to match the refractive index of the glass. The capillary was connected to a glass syringe in a constant displacement pumping system. Solenoids were placed on both sides of the capillary, applying a uniform magnetic field perpendicular to the direction of flow. The solenoids were powered using a Bipolar operational power supply (Kepco BOP 20-5M) and the field strength was monitored with a gauss meter (Lakeshore 425). Optical microscopy (custom column-mounted Nikon, Zyla Andor sCMOS camera) was used to observe the particles during flow in real-time. The objective focused on the mid-plane of the capillary between the solenoids that was 5 cm from the inlet point, where the flow was fully developed.

Dilute solutions ($\text{nL}^3 \ll 1$) of CaP rods suspended in glycerol and IBOA were used with flow rates of 0.05 and 0.5 ml/hr, respectively. The solutions were observed under 0, 400, 600, and 800 Oe (respectively 0, 31831, 47746, 63662 A/m). The length, position, and orientation of fibers within the mid-plane were analyzed 5 cm downstream from the inlet using imaging software (NIS-Elements AR, Nikon).

Results and discussion

Synthesis of CaP Rods

We have demonstrated the ability to fabricate calcium phosphate micro-rods (Fig. 2) that average 50 μm in length and 2 μm in diameter. These anisotropies are very relevant for application as fiber reinforcement in polymers. With high magnification inspection of the rods, the calcium phosphate phase appears to be crystalline exhibiting near-atomic smoothness on the surfaces (Fig. 2B). Crystalline calcium phosphate materials have been shown to exhibit stiffness ranging from 75 - 150 GPa.²¹ Such properties would make these rods very relevant for biocompatible composite materials. Though further analysis of the structure is required, these rods remain intact during severe mixing, centrifugation, and filtration processes.

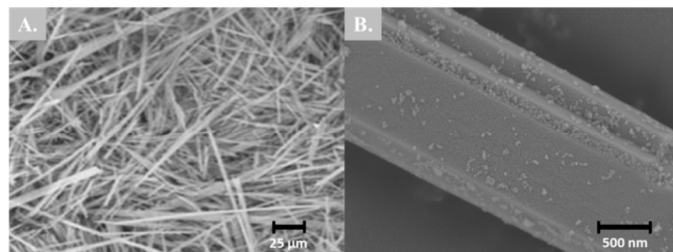


Fig. 2: (A) Scanning electron photomicrograph of calcium phosphate micro-rods synthesized showing the distinct, faceted crystal structure. (B) Scanning electron photomicrograph of calcium phosphate rods after magnetization demonstrates coverage of Fe_3O_4 nanoparticles.

Numerical Validation of Magnetic Energy

To substantiate the analytic expressions for the magnetic torque on a fiber (Eq. 2), a previous numerical model²² has been applied using a Matlab code to predict the rotation of a single, freely rotating CaP fiber suspended in solvent and subjected to a field applied perpendicular to the long axis of the fiber. In rotating to align with the applied magnetic field, the fiber experiences a viscous torque that resists the rotation according to:

$$T_n = -6\eta V \left(\frac{f}{f_0} \right) \left(\frac{d\psi}{dt} \right) \quad (9)$$

The Perrin friction factor for a prolate ellipsoid can be solved analytically using:

$$\frac{f}{f_0} = \frac{4}{3} \frac{1-p^4}{p^2 [aS(2-p^2)-2]} \quad (10)$$

$$S = \frac{2}{A} \frac{1}{\sqrt{1-p^2}} \ln \left(\frac{1 + (\sqrt{1-p^2})}{p} \right)$$

The fiber's angular acceleration can be calculated from Newtonian mechanics as:

$$\frac{d^2\psi}{dt^2} = \frac{T_{\text{net}}}{I} = \frac{5(T_{\text{mag}} + T_n)}{m(A^2 + B^2)} \quad (11)$$

Here m is the mass of the fiber and I is the moment of inertia of an unpinned ellipsoid. Substituting the torques into Eq. 11 leads to a non-

linear, second order differential equation that can be solved using, for example, Matlab. Numerical solutions were compared against experiments, showing good agreement for the predicted rotational velocity and the alignment time (Fig. 3).

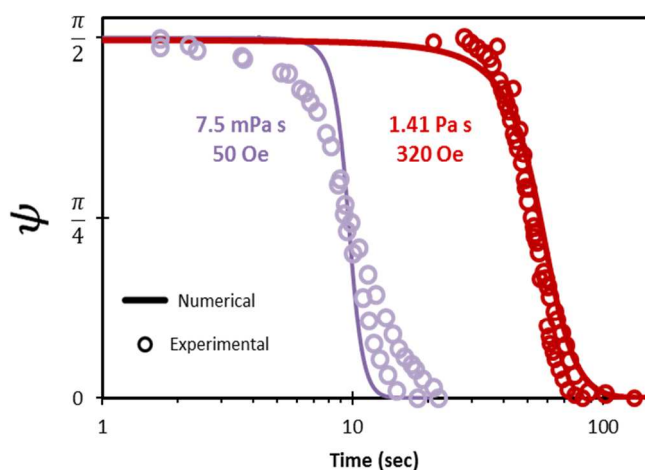


Fig. 3. Comparison between numerical simulations and experimental results of a single rotating fiber suspended in fluids aligning with an external magnetic field. Red curve represents a slow response (solvent of glycerol, $\eta=1.41$ Pa s, $H_0 = 50$ Oe). Purple curve represents a fast response (solvent of IBOA, $\eta=7.5$ mPa s, $H_0 = 320$ Oe).

Since the surface area to volume ratio plays a critical role in the dynamics of the magnetic fibers, the rotational velocity of a rod is influenced primarily by changes in its diameter rather than its length. This allows for the comparison of fibers with slightly variable lengths (20-100 μm) and constant diameters with simulations of a fiber ($A=10$ μm , $B=1$ μm) in glycerol and IBOA. Magnetic fields of 320 Oe (25465 A/m) and 50 Oe (3979 A/m) were used to rotate fibers in glycerol and IBOA, respectively. Image analysis of the fiber rotation experiments was used to measure the average angle vs. time response of the fibers. The maximum predicted angular velocity, which occurs at the angle when the magnetic torque is maximum ($\psi = \pi/4$), of a fiber according to the numerical simulations were 0.04 rad/s and 0.6 rad/s for the glycerol and IBOA based experiments. The average max angular velocities of the fibers measured during the experiments were found to be 0.04 and 0.27 rad/s, respectively.

Experimental Observations of Fiber Alignment under Shear

Using the expression derived for the fiber angle as a function of the flow conditions, fiber geometry, and applied magnetic field (Eq. 8), the predicted angle of a fiber given its geometry and position in the pipe was calculated and compared against the data measured from the experiments. Fig. 4 shows results for experiments conducted under 600 Oe (47746 A/m) for both $\eta = 1.41$ Pa s, $Q = 0.05$ ml/hr and for $\eta = 7.5$ mPa s, $Q = 0.5$ ml/hr. The micrographs in Fig. 4b and 4c correspond to the fibers analyzed in Fig. 4a, and contrast the dominating effect of shear in a high viscosity system as compared to a system with dominating magnetic forces due to lower viscosity.

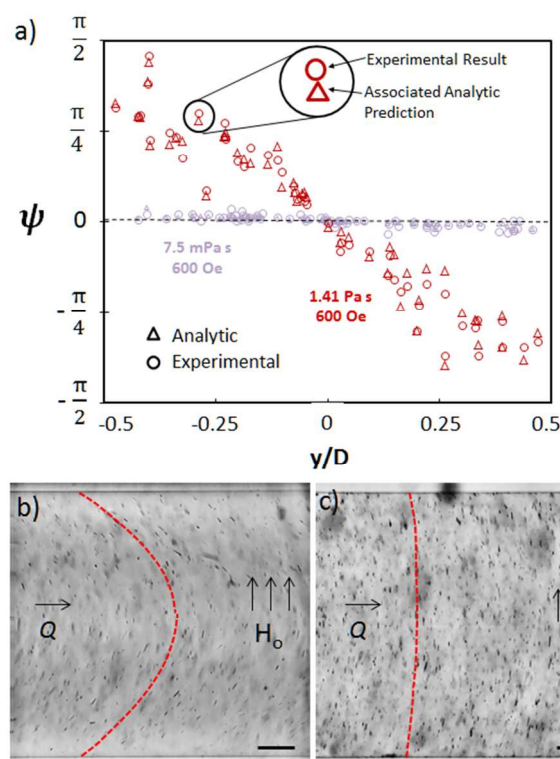


Fig. 4. (a) Comparison of experimental and analytic angle (ψ) vs. distance from the center of the capillary for $\eta=1.41$ Pa s at 0.05 ml/hr (red) and $\eta=7.5$ mPa s at 0.5 ml/hr (purple) with an applied field of 600 Oe. The scatter in the data is due to polydispersity in rod size that is described with the analytic model. Micrographs show associated flow structures for (b) $\eta=1.41$ Pa s and (c) $\eta=7.5$ mPa s. Scale bars are 200 μm .

Comparison of Theory and Experiment

The experiment used for Fig. 4 was repeated for a range of magnetic field strengths (400 Oe to 800 Oe) with for $\eta=1.41$ Pa s at 0.05 ml/hr and $\eta=7.5$ mPa s at 0.5 ml/hr. The position, orientation, and geometry of fibers from each experiment were measured and compared with the analytic model to determine the validity of Eq. 8. Good agreement is illustrated in Fig. 5 between experimental and predicted values for the experimentally observed and analytically predicted orientation of fibers throughout the flow geometries.

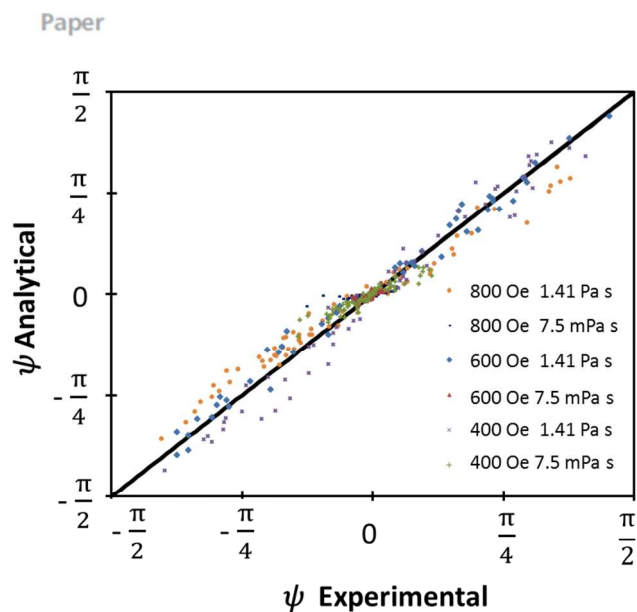


Fig. 5. Comparison shows good agreement between experimental fiber orientations and analytical predictions based on individual fiber geometry, position in the capillary, field strength, flow rate, and viscosity.

The analytic model developed in this work can predict the alignment regimes for different values of the general flow conditions β , which encompasses variable viscosities, flow rates, magnetic field strengths, and magnetic susceptibilities of the fibers (Fig. 6a) as well as for different variable axisymmetric fiber geometries (Fig. 6b). The borderline between phases of good alignment ($\psi = 0^\circ$ - 15°), fair alignment ($\psi = 15^\circ$ - 30°), poor alignment ($\psi = 30^\circ$ - 40°) and bad alignment ($\psi \geq 45^\circ$) is clearly observed in Fig. 6.

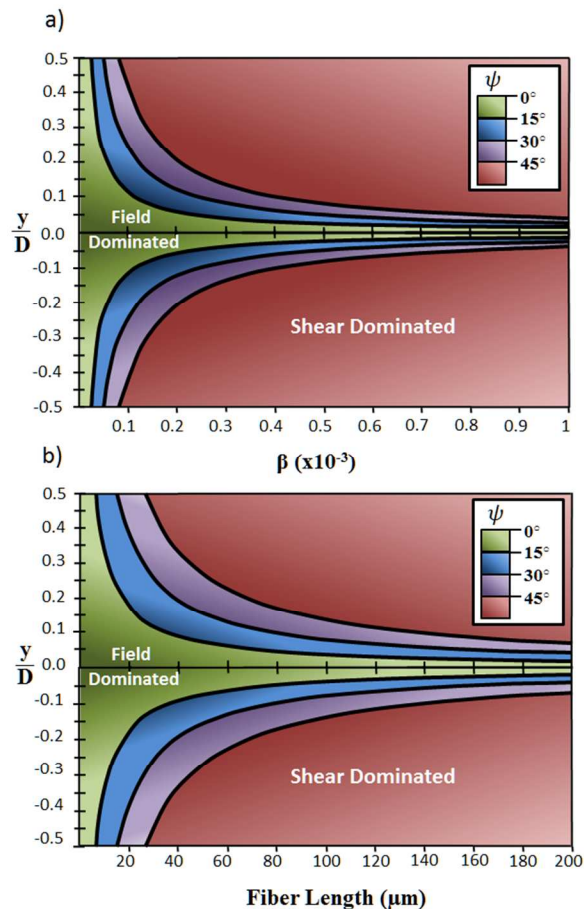


Fig 6. Phase diagrams illustrating the alignment behavior of magnetic fibers throughout the capillary for (a) different values of β with fixed geometry ($A=20 \mu\text{m}$, $B=2 \mu\text{m}$) and for (b) different fiber lengths ($p = 10$), with fixed flow conditions ($\beta = 0.18\text{E-}3$).

Arrestment of Jeffery Orbits

Shear forces have a significant effect of aligning fibers as shown with the large shear-dominated regions in Fig. 6 making this a desired process in techniques from extrusion to tape-casting. However, when fiber suspensions are subject only to shear, the phenomena of Jeffery orbits is created that disrupts perfect alignment in the direction of flow. Since optimized alignment leads to enhanced material properties in these systems, minimizing the effect of Jeffery orbits is critical.

Application of a reasonable magnetic field in these coated fiber suspension under flow completely arrests Jeffery orbits. In the case of applying the field perpendicular to the flow as above (H_o in the direction of $\theta = -\pi/2$), the fibers sit in a stable equilibrium orientation where the aligning magnetic torque balances the misaligning shear torque. Since the fibers are pinned at this orientation, no Jeffery orbits are expected nor observed in experiments.

To gain the optimized alignment in flowing systems desired in many processes, the magnetic field alignment can be tuned to help the shear-induced alignment. Specifically, a magnetic field can be applied along the direction of flow (H_o in the direction of z). To investigate this, a field of 1.2 kOe (95493 A/m) from a handheld rare-earth magnet was

applied in the direction of flow to a dilute solution of fibers in IBOA with a flow rate of 1 ml/hr. Microscopy images in Fig. 7 show the effect of these flow conditions with no applied magnetic field compared to with a strong applied magnetic field. For real time videos, see Supplementary Videos. Jeffrey orbits are clearly and frequently observed in the flow conditions without an applied field. However, when the field is parallel with the flow direction, the Jeffrey orbits get completely arrested due to the pinning effect of the magnetic torque. This technique greatly improves the alignment of fibers by restricting Jeffrey orbits and can be incorporated into current extrusion or tape-casting processes.

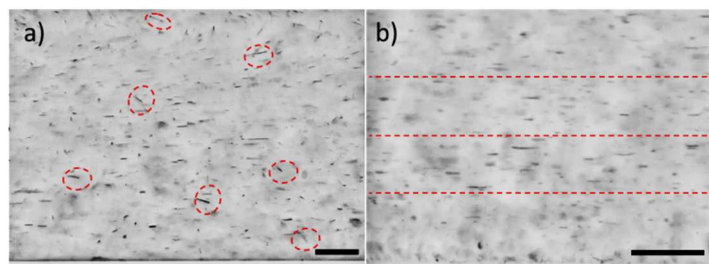


Fig. 7. (a) Flow without an applied field displaying disordered fiber alignments, (b) an applied field applied along the direction of flow restricting Jeffrey orbits, results in excellent fiber alignment. Scale bars are 100 microns.

Conclusions

The theoretical alignment of magnetic fibers in simple shear flow in a capillary was derived using expressions for the magnetic torque and slender body theory for a fiber under shear. The magnetic torque expression was validated with Perrin friction factors for rotating ellipsoids without flow. The analytical model makes excellent predictions of the orientation of fibers taking into a wide number of experimental variables. Applying magnetic torque in these flowing fiber suspensions can be used to overcome shear forces if the fiber length is low, a high applied field is used, or the system is operating at low shear rates. In addition, magnetic torque can be used in tandem with shear-alignment to achieve optimum orientation within a flowing particle suspension. The magnetic torques can work to completely arrest the disordering effect of Jeffrey orbits in these flow conditions. These alignment methods seem to be compatible with current manufacturing technologies including extrusion and tape-casting.

Acknowledgements

We would like to thank Dr. Donald Heiman at Northeastern University for his help with SQUID magnetometry measurements.

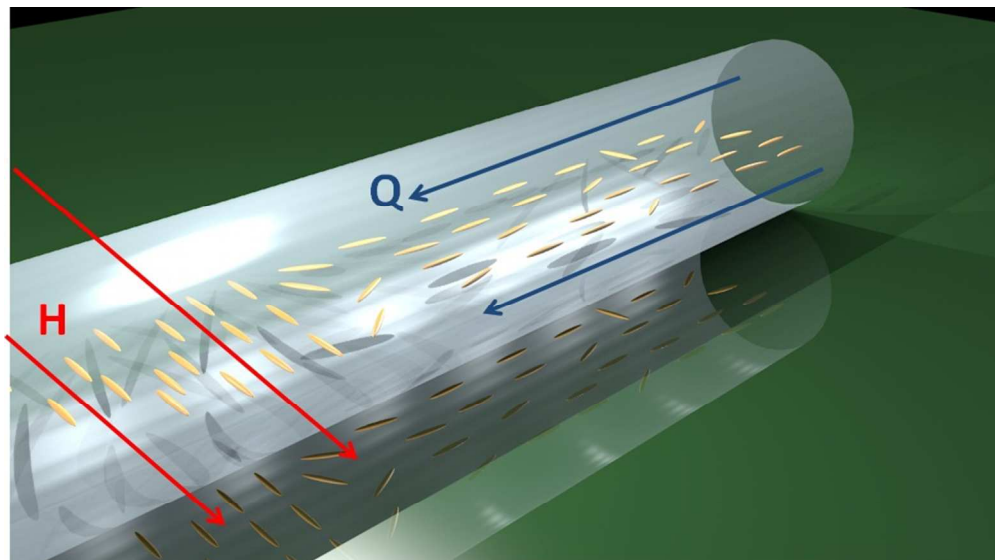
Notes and References

^a Department of Mechanical and Industrial Engineering, Northeastern University, Boston, MA 02115, USA

^b Chemical and Biological Engineering Department, Colorado School of Mines, Golden, CO 80401, USA

1. P. K. Mallick, *Fiber-reinforced Composites: Materials, Manufacturing, and Design.*, CRC Press, 1988.
2. T. D. Papanthasiou, *Flow-induced alignment in composite materials: current applications and future prospects*,

3. Y.-N. Liu, M. Li, Y. Gu, X. Zhang, J. Zhao, Q. Li and Z. Zhang, *Carbon*, 2013, **52**, 550-558.
4. R. Byron Pipes, R. L. McCullough and D. G. Taggart, *Polymer Composites*, 1982, **3**, 34-39.
5. K. H. G. Ashbee, *Fundamental principles of fiber reinforced composites*, Technomic Publishing, 1993.
6. K. Yasuda, T. Kyuto and N. Mori, *Rheol Acta*, 2004, **43**, 137-145.
7. B. G. Compton and J. A. Lewis, *Advanced Materials*, 2014, **26**, 6043-6043.
8. G. B. Jeffery, *Proceedings of the Royal Society of London. Series A*, 1922, **102**, 161-179.
9. R. Libanori, F. H. L. Münch, D. M. Montenegro and A. R. Studart, *Composites Science and Technology*, 2012, **72**, 435-445.
10. R. M. Erb, R. Libanori, N. Rothfuchs and A. R. Studart, *Science*, 2012, **335**, 199.
11. D. Guu, J. K. G. Dhont and M. P. Lettinga, *The European Physical Journal Special Topics*, 2013, **222**, 2739-2755.
12. S. Fraden, G. Maret, D. L. D. Caspar and R. B. Meyer, *Physical Review Letters*, 1989, **63**, 2068-2071.
13. R. G. Cox, *Journal of Fluid Mechanics*, 1970, **44**, 791-810.
14. R. G. Cox, *Journal of Fluid Mechanics*, 1971, **45**, 625-657.
15. G. K. Batchelor, *Journal of Fluid Mechanics*, 1970, **44**, 419-440.
16. G. K. Batchelor, *Journal of Fluid Mechanics*, 1971, **46**, 813-829.
17. F. P. Bretherton, *Journal of Fluid Mechanics*, 1962, **14**, 284-304.
18. C. Ooi, R. M. Erb and B. B. Yellen, *Journal of Applied Physics*, 2008, **103**, -.
19. A. Gómez-Ramírez, P. Kuzhir, M. T. López-López, G. Bossis, A. Meunier and J. D. G. Durán, *Journal of Rheology (1978-present)*, 2011, **55**, 43-67.
20. H. Zhang and B. W. Darvell, *Journal of the American Ceramic Society*, 2011, **94**, 2007-2013.
21. P. Miranda, A. Pajares, E. Saiz, A. P. Tomsia and F. Guiberteau, *Journal of Biomedical Materials Research Part A*, 2008, **85A**, 218-227.
22. R. M. Erb, J. Segmehl, M. Schaffner and A. R. Studart, *Soft Matter*, 2013, **9**, 498-505.



Fiber alignment is the defining architectural characteristic of discontinuous fiber composites and is dictated by shear-dominated processing techniques. Here we study how magnetic alignment can be used to overcome shear, maintain fiber alignment, and arrest Jeffrey orbits.
255x177mm (96 x 96 DPI)